Interarea Oscillation Damping Controls for Wind Power Plants

Mohit Singh, *Member, IEEE*, Alicia J. Allen, *Member, IEEE*, Eduard Muljadi, *Fellow, IEEE*, Vahan Gevorgian, *Member, IEEE*, Yingchen Zhang, *Member, IEEE*, and Surya Santoso, *Senior Member, IEEE*

***Abstract*—This paper investigates the potential for wind power plants (WPPs) to damp interarea modes. Interarea modes may be the result of a single or a group of generators oscillating against another group of generators across a weak transmission link. If poorly damped, these power system oscillations can cause system instability and potentially lead to blackouts. Power conversion devices, particularly, megawatt-scale converters that connect wind turbines and photovoltaic power plants to the grid, could be used to damp these oscillations by injecting power into the system out of phase with the potentially unstable mode. In our model, this power may be provided by a WPP. Over time, the net energy injection is near zero; therefore, providing this "static damping" capability is not expected to affect the energy production of a WPP. This is a measurement-based investigation that employs simulated measurement data. It is not a traditional small-signal stability analysis based on Eigenvalues and knowledge of the power system network and its components. Kundur's well-known two-area, four-generator system and a doubly fed induction generator (DFIG)-based WPP are modeled in PSCAD/EMTDC. The WPP model is based on the Western Electricity Coordination Council (WECC) standard model. A controller to damp interarea oscillations is added to the WECC DFIG model, and its effects are studied. Analysis is performed on the data generated by the simulations. The sampling frequency is set to resemble the sampling frequency at which data are available from phasor measurement units in the real world. The Yule–Walker algorithm is used to estimate the power spectral density of these signals.**

***Index Terms*—Doubly fed induction generators, electromechanical dynamics, interarea oscillations, synchronized phasor measurements, two-area system.**

I. Introduction

WIND penetration levels are increasing throughout the United States. This trend is expected to continue in the following decades [1]. In certain regions of the United States, peak penetration levels can approach 30% [2]. At these penetration levels, in many cases, it is expected that wind power plants (WPPs) will displace conventional generation. This displacement may be permanent as a result of conventional plant retirements based on emissions- or age-related concerns, and because utilities may prefer to install WPPs instead of new conventional generation [3], [4]. Also, recently, load growth is not as high as expected by utilities, while EPA regulations in the US are resulting in older coal plants being retired early. The net result is that there are fewer synchronous machines online. This displacement of conventional synchronous generation by asynchronous WPPs will have significant stability impacts. In this paper, we focus on interarea oscillation modes, in particular. Numerous simulation-based studies have been conducted, with inconclusive results suggesting that the damping of modes may be improved or worsened by wind [5]–[8]. The consensus appears to be that WPPs do not participate directly in oscillation modes; however, their presence leads to the displacement of conventional plant inertia and other topology changes that have the potential to influence the oscillation modes [8]. In these papers, however, the passive effects of wind integration are studied rather than active attempts to damp out oscillations. In this work, we model a familiar two-area test system [9] with an additional WPP. We also add an additional oscillation-damping controller to directly influence modes. The two-area system model is a time-domain model developed using the PSCAD/EMTDC platform [10]. This platform was chosen for its short simulation time-step, giving insight into any dynamics that may appear. This platform has been used earlier for two-area stability analyses [11]. The output from the simulations can be filtered and downsampled to simulate phasor measurement unit (PMU) data. The WPP model is based on the Western Electricity Coordinating Council (WECC) Wind Generator Modeling Group's standard model for Type 3 (doubly fed induction generator, or DFIG) WPPs [12]. The standard model is ported to PSCAD/EMTDC based on the work reported in [13]. Additional controls for interarea oscillation damping have been added to the standard model to inject power into the system out of phase with the potentially unstable mode. A detailed explanation of the model development is provided in Section II.

In the future, long-term PMU data from real power systems can provide information about changes in oscillation modes caused by wind-related or other topology changes. This information could aid planners in evaluating the impacts of proposed generator or line additions. In an environment, in which system data may be frequently changing or may not be readily available, traditional Eigenvalue analysis to find the damping of modes can be challenging. Instead, signal-processing methods can be applied to PMU data to gather information about modes. In this work, a method based on the Yule–Walker algorithm [14] is applied to analyze the simulated PMU data generated by the model. A description of the method is provided in Section III. The effectiveness of the damping controls for different WPP

Manuscript received December 18, 2013; revised June 26, 2014; accepted August 05, 2014. Paper no. TSTE-00541-2013.

M. Singh, A. J. Allen, E. Muljadi, V. Gevorgian, and Y. Zhang are with the Transmission and Grid Integration, National Renewable Energy Laboratory, Golden, CO 80401 USA (e-mail: Mohit.Singh@nrel.gov; alicia.allen@nrel.gov; eduard.muljadi@nrel.gov; vahan.gevorgian@nrel.gov; Yingchen.Zhang@nrel.gov).

S. Santoso is with the Department of Electrical and Computer Engineering, University of Texas at Austin, Austin, TX 73301 USA (e-mail: ssantoso@mail.utexas.edu).

Digital Object Identifier 10.1109/TSTE.2014.2348491

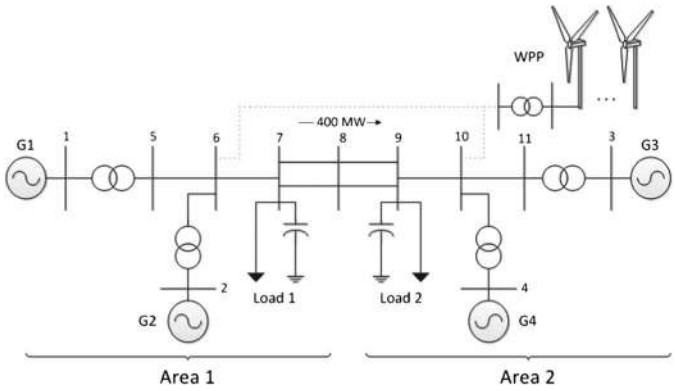

Fig. 1. Two-area system from Kundur [9] with an additional WPP.

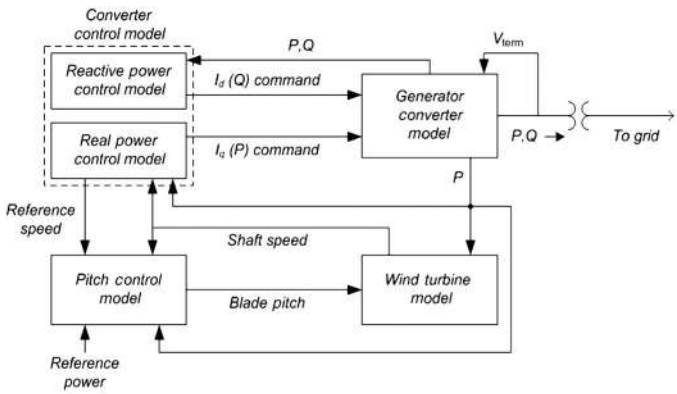

Fig. 2. Schematic of a WECC DFIG WPP model.

output levels is investigated with respect to changes in oscillation modes. These scenarios are discussed in detail in Section IV. The results of the analysis indicate that the oscillation-damping controller is able to influence modes by improving the damping of the system; however, it has to be tuned for one particular mode, and its effects on other modes are difficult to predict. Detailed results and discussion are provided in Section V.

II. Model Development

The model used for these simulations was developed in three stages. In the first stage, a model of the two-area system was developed in PSCAD/EMTDC. In the next stage, a model of the WECC standard WPP was developed and integrated into the two-area system model. The original WECC model was intended for phasor-based modeling software such as PSLF or PSS/E [15]. In our work, we use a time-domain PSCAD/EMTDC equivalent of the WECC model (discussed in detail in [13]). In the third stage, an oscillation-damping controller was developed and added to the model. The software we are using, PSCAD/EMTDC, is typically used for transient analysis, runs at a time step of 10 ms, and thus is more suitable for small-scale systems due to the time taken by each run. We intentionally use this software since we are generating pseudosynchronized phasor measurements using this software that would be difficult to generate using PSS/E, PSLF, or any traditional power system solvers.

A. Two-Area System Model

A one-line diagram of the two-area system is shown in Fig. 1. The base system is symmetrical in terms of generation and line impedance. The model parameters are taken from [9].

In steady-state conditions with no wind, there is a 400-MW transfer from Area 1 to Area 2 across the weak transmission tie between the areas. It should be noted that in our model, power system stabilizers (PSS) and automatic generation control (AGC) are not included; however, each generator's excitation system and governor are modeled. PSCAD/EMTDC parameters for modeling generators and controls not provided in [9] are left at default values when reasonable. For electromechanical transients, reflection of traveling waves at transmission line ends is not important; hence, instead of using traveling-wave or frequency-dependent transmission line models, a coupled-pi transmission line representation is used to model each of the transmission lines in the system.

B. WPP Model

The WPP model is a PSCAD/EMTDC equivalent of the DFIG WPP model developed by the WECC Wind Generator Modeling Group. Fig. 2 illustrates a schematic of the WECC DFIG WPP model framework.

The WPP is sized such that the wind penetration level in the two-area system is 10% when the WPP is supplying rated power. The WPP collector system model is represented by an aggregated single-line equivalent. Details on how this aggregation is performed are provided in [16]. The collector system data for the aggregation process are from a real WPP and are presented in [16]. The WECC DFIG WPP model is well documented, and parameters for the model are available [15].

C. Oscillation Damping WPP Controls

Additional WPP controls may be provided by the turbine manufacturer for the purpose of frequency support, but no manufacturer yet offers a dedicated oscillation damping control. Typical frequency support controls include governor droop control and synthetic inertia. Detailed explanations of droop control and synthetic inertia are provided in [17]–[22]. The effects of these controls on oscillation modes are unknown. These controls are not considered in our modeling effort because they are nonstandard additions to the WECC WPP model and its effect on modal behavior is debatable.

Oscillation damping controls also differ from frequency support controls in one major aspect: energy injection. The goal of the oscillation damping control is to have a near-zero injection of energy during the time frame of controller action. This means that unlike in the case of frequency support controls, the WPP operator does not suffer much revenue loss during controller action.

In our test case, the WPP is connected at Bus 6 (see Fig. 1). An optional connection at Bus 10 is not utilized, thus the WPP is supplying only Area 1 directly. The power at the wind turbine's point of interconnection (Bus 6 in our test case) is

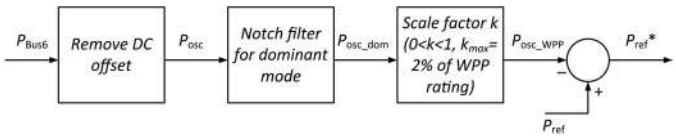

Fig. 3. Control block diagram of oscillation damping control.

measured by the PMU. The damper is tuned to the dominant interarea modal frequency (0.76 Hz in our test system). When this frequency is observed in the local WPP PMU measurements, the controller is activated. Often, good wind resource areas (areas with high wind speeds all year round, affordable land, and available transmission) are situated far from load centers. This situation is seen especially in the Western United States and Texas. In the Western United States, some of the best wind resource is in Wyoming, where there are no major load centers nearby at all. In Texas, West Texas has the best wind resource but the large load centers are hundreds of miles away. Area 1 in our model represents the wind-resource-rich area, while Area 2 represents the faraway load center. This is the reason we have opted for the connection at Bus 6 instead of 10.

The implementation of the oscillation damping controller is shown in Fig. 3. The power at Bus 6 is our measured variable, supplied by a simulated PMU at the point of interconnection. In the real world, a PMU at the point of interconnection of the WPP would supply this information. In our work, this data are supplied to the WPP in the form of pseudosynchronized phasor measurements. Removing the DC component of this power leaves us with the oscillatory component. Applying a notch filter tuned to 0.76 Hz to the oscillatory component allows isolation of the dominant oscillation mode. We scale down the oscillatory component (so as not to exceed converter ratings for the turbines; see Section V) and add the inverse of this scaled oscillatory component to the reference power command of the WPP (Fig. 2 shows where this reference power is inputted into the model). Thus, the WPP will oppose the oscillation. It is expected that the WPP controller will then assign power commands to individual turbines; however, the WECC WPP model does not include individual turbine representations so individual turbine behavior is not modeled. This proposed oscillation damping controller only has a proportional component, and no integral or derivative component. To tune the proportional gain, the traditional Ziegler–Nichols method has been employed. This method of tuning results in aggressive gain and overshoot. Future work will optimize this controller based on a cost function that will include wind turbine load reduction; however, this is beyond the scope of the present work.

Most large power systems only have a few interarea modes that are potentially unstable. Of these few modes, the WPP can at most affect one, since likely only one mode will be predominant in the WPP's area. For example, the North–South mode (0.318 Hz) in the WECC system cannot be damped by a wind turbine outside these two areas. Thus, damping of the predominant mode is the focus in this paper. Note also that while in the WECC-developed model shown, the entire plant is modeled as one entity; in real life, the individual turbines will have to perform the work. Unlike inertial response which is achieved by programming each turbine's controller, here it is necessary that the WPP controller assigns commands. This is because only the WPP controller will have access to the PMU data about the oscillations, since there is only one PMU for the plant and not one for each turbine. As a contrast, each turbine can measure the frequency at its own terminals and can determine whether to supply inertial response or not.

III. Simulated Phasor Data Processing

Synchronized phasor measurements are high-precision time-synchronized measurements that have the ability to provide information on an interconnected power system's electromechanical modal behavior. Electromechanical modal information consists of modal frequencies and damping and mode shape. This information is extracted from synchronized phasor measurements using signal-processing methods that are described in this section. Pseudosynchronized phasor measurements are created using the simulated two-area system described in Section II. These pseudosynchronized phasor measurements are also high precision and time-synchronized and are thus similar to real power system measurements taken by PMUs. The advantage of using the simulated system instead of real data is that changes to the system (such as changes to generator inertia or WPP location) can be made and their effects on modal behavior can then be studied. The number of observations per second is also higher in the pseudosynchronized phasor measurements. The pseudomeasurements are filtered and downsampled to the typical 30 observations per second for PMU measurements [23].

In this paper, two signal-processing methods are used to extract modal information from the pseudosynchronized phasor measurements. The first, the matrix-pencil (MP) method [24], [25], is a linear, time-domain method that fits a linear model to the evenly spaced pseudomeasurements. The MP method is used to estimate the modal frequencies and damping that are present in the system. For the second, the power spectral density (PSD) is estimated based on autoregressive (AR) model fitting using the Yule–Walker (YW) method [25]. For the AR YW method, the signal examined is assumed to be the output of a system that is driven by white noise [14]. The PSD provides a visual representation of the strengths of the modal frequencies present in the pseudomeasurements. Significant peaks in the PSD indicate dominant frequencies present in the measurements. Results of these methods applied to pseudomeasurements for a number of different cases are provided in Section V.

IV. Simulation Cases

Simulations were performed in four configurations with respect to wind power output level and oscillation damping controller status (enabled or disabled). The cases are listed in Table I. Each of the synchronous units G1 through G4 is assumed to be a perfectly coherent representation of multiple synchronous generators. The presence of wind leads to the displacement of conventional units, hence leading to a reduction in the number of machines making up a coherent unit. This is represented in our simulation by a reduction in the inertia of coherent unit G2, which is closest to Bus 6, the point of

TABLE I
LIST OF CASES BASED ON WIND POWER OUTPUT, WIND LOCATION, AND INERTIA REDUCTION LOCATION

Case no.	Wind power output (pu)	Oscillation damper control status
1	0.5	Disabled
2	0.5	Enabled
3	1.0	Disabled
4	1.0	Enabled

interconnection of the WPP. The decision to reduce inertia on this coherent unit to a third of its original value represents the removal of turbogenerators (typical inertia 3–9 s) from a coherent unit, whereas hydrounits (typical inertia 2 s) remain [26]. Two wind power output levels were considered: 0.5 and 1 p.u. If wind power output was to be at 0 p.u., the provision of the oscillation damping service would be impossible; some stored energy in the rotating masses of the turbines is necessary to provide this service.

V. RESULTS

Results from the case studies are presented here. The simulated two-area system is excited by a large disturbance—a breaker connecting an impedance load in parallel to Load 2 located at Bus 9 in Fig. 1 is suddenly switched ON. The additional load is 1% of Load 2 in terms of real and reactive power. The signal-processing methods described in Section III are applied to the resulting electromechanical oscillations to estimate the modal frequency, damping, and the mode shape of the system. The estimated modes for each case are compared to determine if the WPP output levels or the controller status influence the system modes.

A. Power Spectral Density Analysis

For the case studies, the frequency at each generator bus, the voltage phase angle with respect to the calculated center of angle [9], the voltage phase angle at each generator bus, and the power output at each generator were used to estimate the modes of the system after the power system disturbance was applied. The results of the analysis on the power output at each generator are presented in Figs. 4–7. The power output signal was selected to analyze modes because the mode estimates were clearest for this signal compared to the voltage phase angle and frequency signals. Note that the modal content in the two areas is not identical because load in the two areas is asymmetrical.

In Fig. 4, the significant peaks in the PSD indicate modal frequencies present in the power output at generator G1 located at Bus 1 for all cases. The top of Fig. 4 shows the PSD for wind output at 0.5 p.u. (Case 1 and Case 2). The bottom of Fig. 4 shows the PSD for wind output at 1 p.u. (Case 3 and Case 4). All of these plots indicate the presence of 0.76 Hz, both with the damping controller disabled and with it enabled. This 0.76-Hz

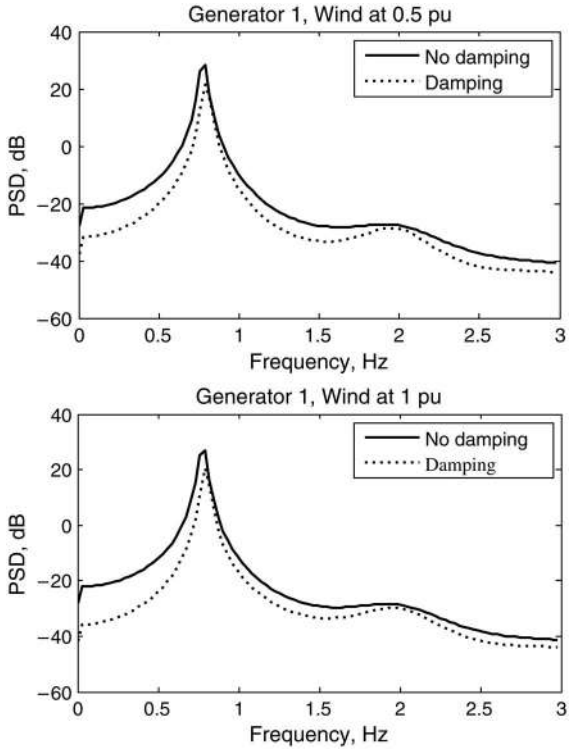

Fig. 4. Yule–Walker PSD estimates for the G1 power signal.

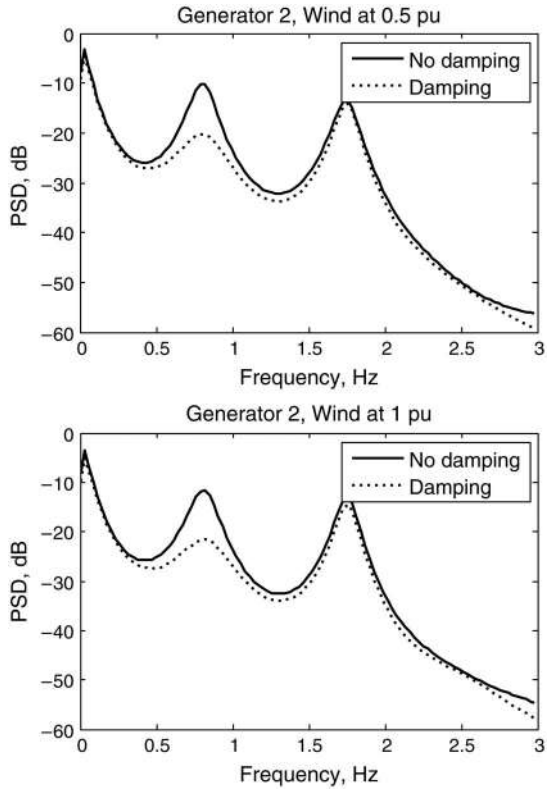

Fig. 5. Yule–Walker PSD estimates for Generator G2 power signal.

frequency falls in the interarea oscillation range (0.1–0.8 Hz) [27], indicating that this frequency is associated with one group of generators oscillating against another group of generators in the system. The presence of the damping controller reduces

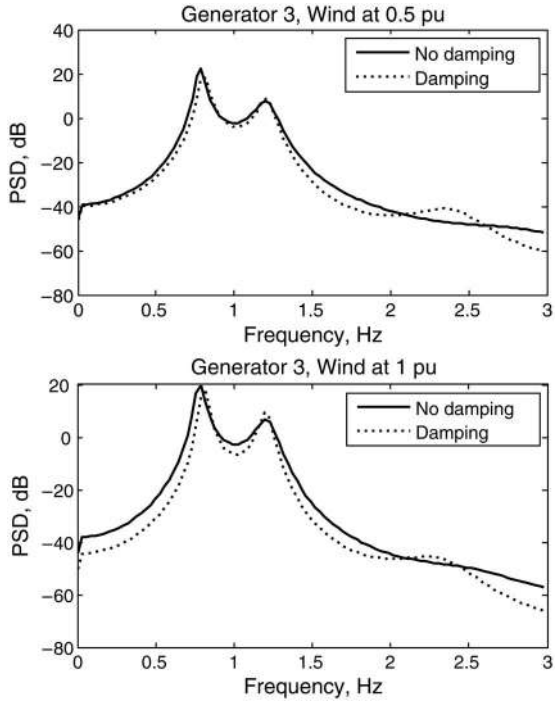

Fig. 6. Yule–Walker PSD estimates for the G3 power signal.

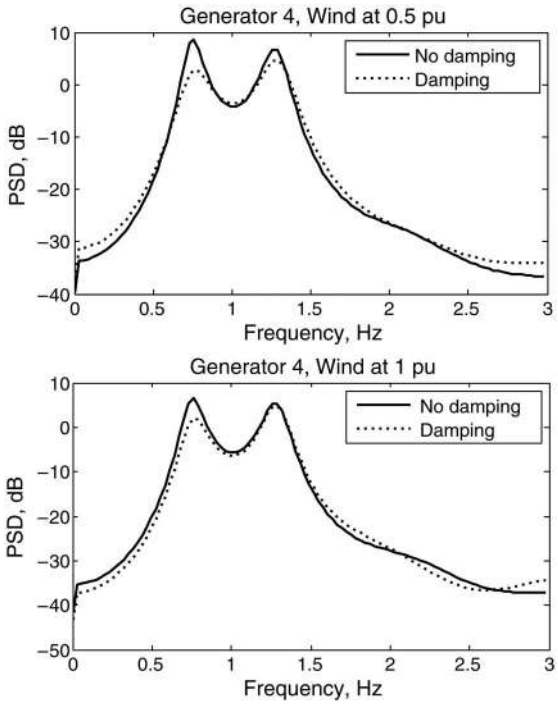

Fig. 7. Yule–Walker PSD estimates for the G4 power signal.

the peak magnitude of the 0.76-Hz mode by approximately 7 dB when the wind output is at 0.5 p.u. and by approximately 5 dB when the wind output is at 1 p.u. This reduction in the mode's peak magnitude indicates that the damping controller is indeed performing its function. The damping controller cannot eliminate the mode entirely because of the small amount of power that it can supply (limited to 2% of the WPP's rating) compared to the power involved in the interarea oscillation. The lack of significant additional peaks when wind power is changed from 0.5 to 1 p.u. indicates that the WPP output levels investigated *do not* have a direct impact on the modes of the system.

The same cases are studied in Fig. 5, but the power output of G2 located at Bus 2 is analyzed. The PSD results are shown. In addition to the 0.76-Hz mode, a DC component as well as a modal frequency at 1.75 Hz is visible as significant peaks. Frequencies in this range are associated with intraarea oscillations (0.7–2.0 Hz)—when a single generator oscillates against another generator or group of generators [27]. The intraarea oscillation at 1.75 Hz is caused by the generators 1 and 2 interacting with each other. This oscillatory mode is also excited by the load disturbance. However, intraarea modes are of less concern due to the proximity of the generators; the absence of long lines means that the damping of these modes is usually much higher than for interarea modes and the potential for instability is much lower. The top of Fig. 5 shows the PSD for wind output at 0.5 p.u. (Case 1 and Case 2). The bottom of Fig. 5 shows the PSD for wind output at 1 p.u. (Case 3 and Case 4). All of these plots again indicate the presence of 0.76 Hz, both with the damping controller disabled and with it enabled. The presence of the damping controller reduces the peak magnitude of the 0.76-Hz mode by approximately 10 dB when the wind output is at 0.5 p.u. and by approximately 9 dB when the wind output is at 1 p.u. This reduction in the mode's peak magnitude again indicates that the damping controller is performing its function. Because the coherent unit G2 is electrically closer to the WPP, the controller's damping effects appear to be more pronounced than in the G1 power signal. The inference can be made from this fact that the proximity of a coherent unit to the WPP indicates how well the controller will damp oscillations at that unit's terminals.

Fig. 6 shows the PSD for unit G3 at Bus 3 in Area 2. For G3, aside from the 0.76-Hz mode, an additional significant peak occurs at 1.17 Hz. Although the 0.76-Hz mode appears to be damped better (approximately 3 dB lower peaks) with the oscillation damper enabled for both the 0.5- and 1-p.u. output cases, the 1.17-Hz mode appears unaffected. G3 is the farthest from the WPP electrically, and the fact that the damping effect of the controller is much weaker here than it is for G2 seems to indicate that our hypothesis about the proximity of a unit to the WPP leading to improved damping is correct. Fig. 7 shows the PSD for G4 at Bus 4 in Area 2. Again, aside from the 0.76-Hz mode, an additional significant peak occurs at 1.17 Hz. Although the 0.76-Hz mode appears to be better damped (approximately 7 dB lower peaks) with the oscillation damper enabled for both the 0.5- and 1-p.u. output cases, the 1.17-Hz mode appears unaffected. G4 is much closer than G3 to the WPP electrically, and the fact that the damping effect of the controller is better here than it is for G3 again seems to confirm that our hypothesis about the proximity of a unit to the WPP leading to improved damping is correct.

B. MP Analysis Technique

The effectiveness of the damping controller is measured using another technique in this section. The MP method is used

TABLE II
FREQUENCY AND DAMPING ESTIMATES FOR 0.76-HZ MODE

Generator	Case	Frequency (Hz)	Damping (%)
G1	1	0.77	0.41
	2	0.80	1.49
	3	0.77	0.42
	4	0.80	1.70
G2	1	0.77	0.55
	2	0.79	1.37
	3	0.77	0.41
	4	0.80	1.40
G3	1	0.78	0.46
	2	0.80	1.56
	3	0.78	0.71
	4	0.80	2.06
G4	1	0.78	0.58
	2	0.80	1.75
	3	0.78	0.89
	4	0.80	2.41

to estimate the modal frequency and damping in each generator's power output for all four cases. The difference between the methods is that the MP method is a parametric method while the Yule–Walker PSD method is classified as a spectral method. The two methods use different mathematical techniques to derive mode estimates [14]. In our work, the MP method is used to confirm results from the Yule–Walker PSD method. Using two methods that are mathematically different but are in agreement gives a better likelihood of the mode being estimated correctly. Table II shows the frequency and damping estimates for all four generators for each case. The interarea 0.76-Hz mode is the only one studied in this analysis. The 0.76-Hz mode shifts to approximately 0.8 Hz whenever the damping controller is enabled. This is less visible in the Yule–Walker PSD plots in Figs. 4–6; however, a rightward shift of this mode is discernable even in those figures. This is a result of a change in the overall structure of the system due to the additional control loop introduced by the damping controller. The damping estimates for all these cases indicate that the 0.76-Hz mode is better damped for cases when the damping controller is enabled (the damping in percent is approximately thrice that without the damping controller). Thus, this analysis provides further proof and confirmation of the damping controller's effectiveness.

C. Net Energy Injection and Cost of Service

Fig. 8 shows the WPP output during the controller action time frame. When the controller is disabled, the WPP output does not deviate from the commanded value. When the controller is enabled, the controller opposes the dominant oscillation mode by injecting energy out of phase with the oscillation.

To determine how much energy the controller injects, it is useful to find the area under the curve for each case. Our WPP model is based on a plant with 135 1.5-MW turbines, for a combined plant rating of 204 MW. For the cases when wind power output is at 0.5 p.u., the area under the curve yields

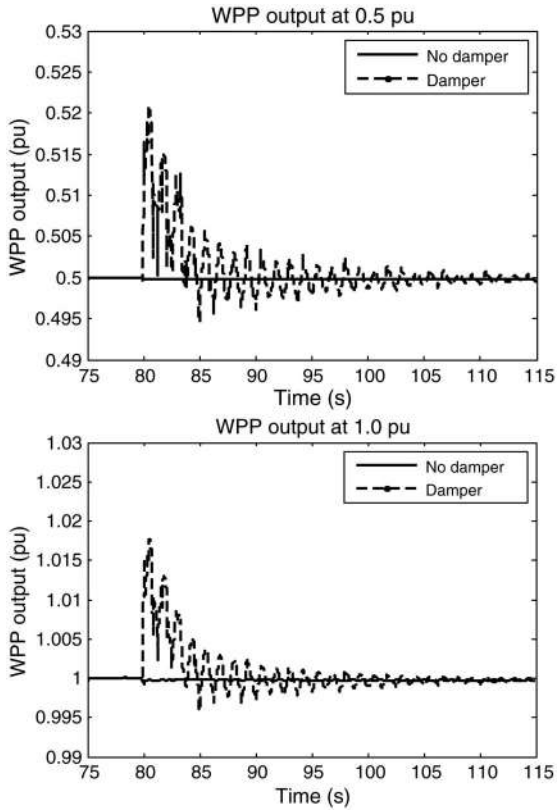

Fig. 8. WPP output during controller action time frame with controller disabled and enabled (for the 0.5- and 1-p.u. output cases).

3960.1 MW-s with controller disabled, and 3968.1 MW-s with controller enabled. This implies that the controller used an additional 8 MW-s during the time frame of controller action. This number (8 MW-s) is the same for the 1-p.u. output case. This additional energy must come from the stored energy of the turbines. Because a turbine's inertia time constant is usually in the order of 4 s, a 1.5-MW turbine has 4×1.5 MW-s or 6 MW-s stored. Throughout a plant of 135 turbines, this equates to 810 MW-s of stored energy. Thus, 8 MW-s equates to approximately only 1% of the energy stored in the plant's rotating inertia, and the plant can easily supply this with no noticeable impact on operation. In terms of revenue, assuming a levelized cost of energy from wind of 50 dollars per MWh [1], each controller operation will cost only approximately 11 cents. Even if the controller operates 100 to 1000 times in a year, the cost of providing this service is negligible compared to the plant's revenue. Because the impact on stored energy is so small, it is not expected that controller action will have noticeable impacts on turbine wear and tear or reliability. We will attempt to quantify the reliability impacts in future work.

D. Effect of Increase in Penetration Level

Since a 10% penetration level may be considered relatively low for future systems, a 20% penetration case was considered as well. A Yule–Walker PSD analysis was carried out for this penetration level. The PSD for generator G1, at 1 p.u. output, for a 20% penetration case is shown in Fig. 9. The damping controller's performance is improved compared to the performance

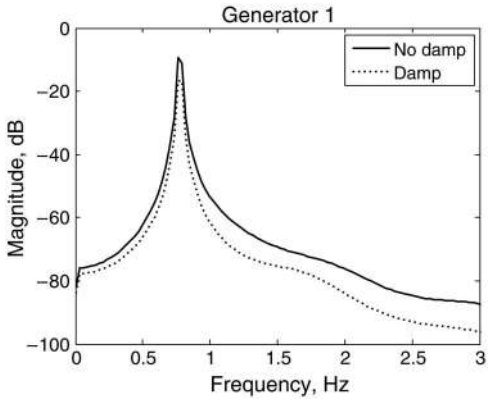

Fig. 9. Yule–Walker PSD estimates for the G1 power signal (output, 1 p.u.).

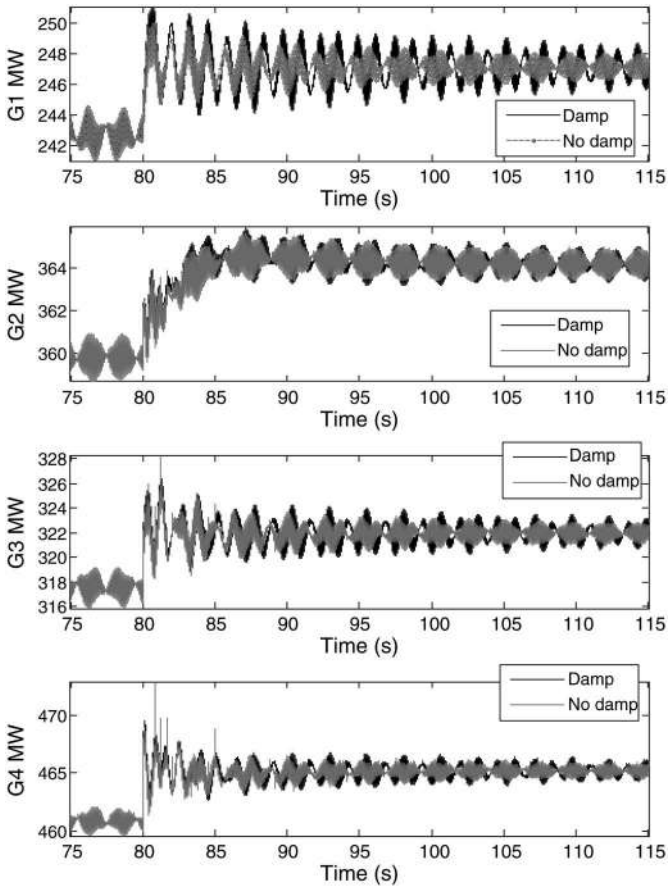

Fig. 10. Power signal (wind output, 1 p.u.) for all four generators with and without damper.

seen in Fig. 4. Additionally, it appears that the mode is better damped in general due to the higher percentage of power coming from an asynchronous source.

In the previous sections, our emphasis was on showing that damping of interarea modes is possible using wind plant control even at relatively low penetration levels such as seen today in the United States. With higher penetration levels, the controller will have more stored energy at its disposal and thus will be able to damp oscillations more easily, as shown by the 20% penetration case.

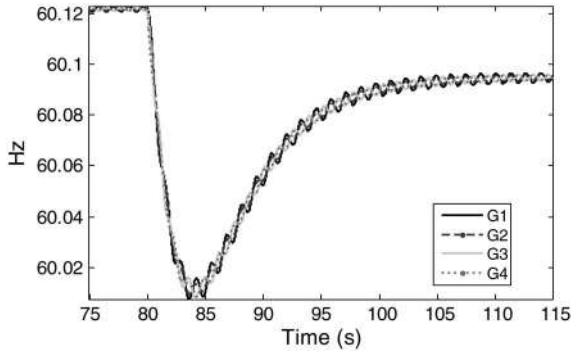

Fig. 11. Frequency signal (wind output, 1 p.u.) for all four generators without damper.

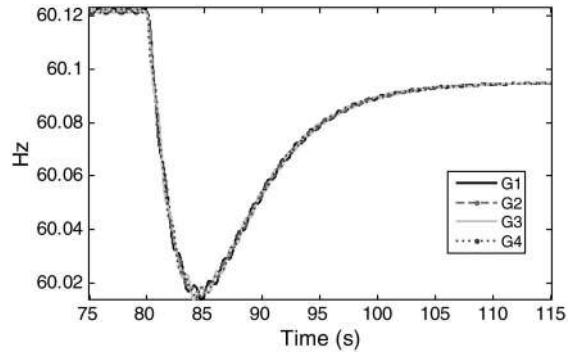

Fig. 12. Frequency signal (wind output, 1 p.u.) for all four generators with damper.

E. Visibility of Damping Effects in Time Domain

While the damping effect caused by the controller is easily visible in the frequency domain, it is also visible in the time domain, as shown in Fig. 10. In this figure, the power output of each synchronous generator is shown during the load disturbance. Output of the wind plant is set to 1 p.u. However, it is difficult to calculate the degree of damping numerically in the time domain, and thus frequency domain methods provide a better insight into the level of damping.

Figs. 11 and 12 show the frequency plots for all four generators. In Fig. 11, the damper is disabled, and in Fig. 12, the damper is enabled. From visual inspection, it is possible to see that the damping is indeed better with the damper enabled. Once again, however, it is difficult to use these plots to generate a numerical comparison.

VI. Conclusion

The work shown here indicates that WPPs can make a contribution to the damping of interarea oscillation modes. A controller has been developed that allows WPPs to inject power into the system out of phase with the interarea oscillation to increase the damping of the oscillation. The controller is able to increase the damping of the oscillation but performs better at damping oscillations at nearby generators. The cost to the WPP operator of providing this service appears to be negligible; however, further work will determine reliability impacts of deploying this controller to better inform WPP operators'

TABLE III
SCRX EXCITER FOR ALL FOUR GENERATORS

Parameter	Value
Rectifier smoothing time constant	0.02 s
Controller lead time constant	1.5 s
Controller lag time constant	1 s
Exciter time constant	0.02 s
Exciter gain	100
Max. field voltage	5 pu
Min. field voltage	−5 pu
L-G voltage base	11.55 kV
Line current base	45 kA
Reverse resistance	15 000 Ω
Exciter voltage supply	Independent
4-Quadrant operation	No

TABLE IV
IEEE TYPE 2 GOVERNOR DATA FOR ALL FOUR GENERATORS

Parameter	Value
Controller real pole gain	0.88
Controller proportional gain	3.7
Controller integral gain	0.44
Controller real-pole time constant	0.02 s
Turbine lead time constant	0.01 s
Turbine lag time constant	0.01 su
Governor time constant	0.05 s
Inverse gate velocity limit	4.8 s/pu
Gate velocity time constant	0.1 s
Permanent droop gain	0.08
Gate position rate control limit	0.22 pu/s
Temporary droop gain	0.0
Temporary droop time constant	0.01 s
Conversion constant	0.895
Time constant for smoothing	0.02 s

and system operators' decisions. The primary benefit of the analysis technique described in this paper is that network data need not be known. In future work, these results will be validated using archived PMU data from real power systems and using the capabilities of NREL's controllable grid interface. In the future, by providing this service, WPPs could play an active role in improving the grid's stability. As wind penetration levels increase, such analyses will become increasingly relevant.

APPENDIX
EXCITER AND GOVERNOR DATA FOR TWO-AREA SYSTEM

The excitation system is identical for all four generators. The excitation system for all four generators is the silicon-controlled rectifier (SCR) bridge type exciter, modeled using the PTI SCRX model. The block diagram is available in [28]. The data for the exciters are provided in Table III.

For active power control, all four employ IEEE Type 2 hydro governors, for which the block diagram is available in [29]. The data for the governors are provided in Table IV.

All the other data for the generators can be found in [9], and the data for the WPP can be found in [13] and [15].

REFERENCES

[1] DOE, "20% wind energy by 2030: Increasing wind energy's contribution to U.S. electricity supply," National Renewable Energy Lab., Golden, CO, USA, Tech. Rep. NREL/TP-500-41869, DOE/GO-102008-2567, May 2008 [Online]. Available: www.nrel.gov/docs/fy08osti/41869.pdf

[2] Electric Reliability Council of Texas, "ERCOT grid operations wind integration report: 05/02/2013," Electric. Reliability Council of Texas, Austin, TX, USA, 2013 [Online]. Available: http://www.ercot.com/content/gridinfo/generation/windintegration/2013/05/ERCOT%20Wind%20Integration%20Report%2005-02-13.pdf

[3] GE Energy, "Western wind and solar integration study," National Renewable Energy Lab., Golden, CO, USA, Subcontract Rep. NREL/SR-550-47434, 2010 [Online]. Available: http://www.nrel.gov/docs/fy10osti/47434.pdf

[4] N. Miller, M. Shao, and S. Venkataraman, "CAISO frequency response study," GE Energy, Schenectady, NY, USA, 2011 [Online]. Available: http://www.uwig.org/Report-FrequencyResponseStudy.pdf

[5] J. G. Slootweg and W. L. Kling, "The impact of large-scale wind power generation on power system oscillations," *Electr. Power Syst. Res.*, vol. 67, pp. 9–20, 2003.

[6] G. Tsourakis, B. M. Nomikos, and C. D. Vournas, "Contribution of doubly-fed wind generators to oscillation damping," *IEEE Trans. Energy Convers.*, vol. 24, no. 3, pp. 783–791, Sep. 2009.

[7] A. Mendonca and J. A. Peas Lopes, "Impact of large-scale wind power integration on small-signal stability," in *Proc. Int. Conf. Future Power Syst.*, Nov. 2005.

[8] D. Gautam, V. Vittal, and T. Harbour, "Impact of increased penetration of DFIG-based wind turbine generators on transient and small-signal stability of power systems," *IEEE Trans. Power Syst.*, vol. 24, no. 3, pp. 1426–1434, Aug. 2009.

[9] P. Kundur, *Power System Stability and Control*. New York, NY, USA: McGraw-Hill, 1974, p. 814.

[10] Manitoba HVDC Research Centre, "PSCAD/EMTDC: Electromagnetic transients program including dc systems," 1994.

[11] T. K. Das and G. K. Venayagamoorthy, "Optimal design of power system stabilizers using a small population based PSO," in *Proc. IEEE Power Eng. Soc. Gen. Meeting*, Montreal, QC, Canada, Jun. 12–16, 2006.

[12] M. Behnke *et al.*, "Development and validation of WECC variable-speed wind turbine dynamic models for grid integration studies," in *Proc. WINDPOWER Conf.*, Los Angeles, CA, USA, Jun. 2007.

[13] M. Singh and S. Santoso, "Dynamic models for wind turbines and wind power plants," National Renewable Energy Lab., Golden, CO, USA, Subcontract Rep. NREL/SR-52780, 2011 [Online]. Available: http://www.nrel.gov/docs/fy12osti/52780.pdf

[14] J. W. Pierre, D. J. Trudnowski, and M. K. Donnelly, "Initial results in electromechanical mode identification from ambient data," *IEEE Trans. Power Syst.*, vol. 12, no. 3, pp. 1245–1251, Aug. 1997.

[15] WECC Renewable Energy Modeling Task Force, "WECC wind power plant dynamic modeling guide," 2010 [Online]. Available: http://renew-ne.org/wp-content/uploads/2012/05/WECCWindPlantDynamicModelingGuide.pdf

[16] E. Muljadi *et al.*, "Equivalencing the collector system of a large wind power plant," in *Proc. IEEE Power Eng. Soc. Gen. Meeting*, Montreal, QC, Canada, Jun. 12–16, 2006.

[17] G. Lalor, A. Mullane, and M. O'Malley, "Frequency control and wind turbine technologies," *IEEE Trans. Power Syst.*, vol. 20, no. 4, pp. 1905–1913, Nov. 2005.

[18] G. Ramtharan, J. B. Ekanayake, and N. Jenkins, "Frequency support from doubly-fed induction generator wind turbines," *IET Renew. Power Gener.*, vol. 1, pp. 3–9, 2007.

[19] J. F. Conroy and R. Watson, "Frequency response capability of full-converter wind turbine generators in comparison to conventional generation," *IEEE Trans. Power Syst.*, vol. 23, no. 2, pp. 649–656, May 2008.

[20] N. R. Ullah, T. Thiringer, and D. Karlsson, "Temporary primary frequency control support by variable-speed wind turbines—Potential and applications," *IEEE Trans. Power Syst.*, vol. 23, no. 2, pp. 601–612, May 2008.

[21] A. Buckspan, J. Aho, P. Fleming, Y. Jeong, and L. Pao, "Combining droop curve concepts with control systems for wind turbine active power control," in *Proc. IEEE Power Electron. Mach. Wind Appl. (PEMWA)*, Denver, CO, USA, Jul. 2012.

[22] J. Morren, S. W. H. De Haan, W. L. Kling, and J. A. Ferreira, "Wind turbines emulating inertia and supporting primary frequency control," *IEEE Trans. Power Syst.*, vol. 21, no. 1, pp. 433–434, Feb. 2006.

[23] I. Kamwa, A. K. Pradhan, and G. Joos, "Adaptive phasor and frequency-tracking schemes for wide-area protection and control," *IEEE Trans. Power Del.*, vol. 26, no. 2, pp. 744–753, Apr. 2011.

[24] T. K. Sarkar and O. Pereira, "Using the matrix pencil method to estimate the parameters of a sum of complex exponentials," *IEEE Antennas Propag. Mag.*, vol. 37, no. 1, pp. 48–55, Feb. 1995.

[25] M. Bounou, S. Lefebvres, and R. P. Malhame, "A spectral algorithm for extracting power system modes from time recordings," *IEEE Trans. Power Syst.*, vol. 7, no. 2, pp. 665–683, May 1992.

[26] G. Andersson, R. Atmuri, R. Rosenqvist, and S. Torseng, "Influence of Hydro Units' generator-to-turbine inertia ratio on damping of subsynchronous oscillations," *IEEE Trans. Power App. Syst.*, vol. PAS-103, no. 8, pp. 2352–2361, Aug. 1984.

[27] M. Klein, G. J. Rogers, and P. Kundur, "A fundamental study of inter-area oscillations in power systems," *IEEE Trans. Power Syst.*, vol. 6, no. 3, pp. 914–921, Aug. 1991.
[28] F. P. De Mello, P. J. Nolan, T. F. Laskowski, and J. M. Undrill, "Coordinated application of stabilizers in multimachine power systems," *IEEE Trans. Power App. Syst.*, vol. PAS-99, no. 3, pp. 892–901, May 1980.
[29] Working Group on Prime Mover, and Energy Supply Models for System Dynamic Performance Studies, "Hydraulic turbine and turbine control models for system dynamic studies," *IEEE Trans. Power Syst.*, vol. 7, no. 1, pp. 167–179, Feb. 1992.

Mohit Singh (M'11) received the M.S. and Ph.D. degrees in electrical engineering from the University of Texas at Austin, Austin, TX, USA, in 2007 and 2011, respectively.

He is currently working as an Engineer in transmission and grid integration of renewable energy with the National Renewable Energy Laboratory, Golden, CO, USA. His research interests include the dynamic modeling of wind turbine generators, modeling and testing various applications of wind turbine generators, and other renewable energy resources.

Dr. Singh is involved in the activities of the IEEE Power and Energy Society.

Alicia J. Allen (M'13) received the Ph.D. degree in electrical engineering from the University of Texas at Austin, Austin, TX, USA, in 2013.

She joined the transmission and grid integration group, National Renewable Energy Laboratory, Golden, CO, USA, in April 2013.

Her research interests include power system impacts of the integration of MW-scale wind turbines on the distribution system, wide-area measurement and control systems, power system protection, and power system stability.

Eduard Muljadi (M'82–SM'94–F'10) received the Ph.D. degree in electrical engineering from the University of Wisconsin, Madison, WI, USA.

From 1988 to 1992, he taught at California State University, Fresno, CA, USA. In June 1992, he joined the National Renewable Energy Laboratory, Golden, CO, USA. His research interests include electric machines, power electronics, and power systems, in general, with emphasis on renewable energy applications.

Dr. Muljadi is a member of Eta Kappa Nu and Sigma Xi. He is involved in the activities of the IEEE Industry Application Society (IAS), Power Electronics Society, and Power and Energy Society (PES). He is currently a member of various committees of the IAS, a member of Working Group on Renewable Technologies and Dynamic Performance Wind Generation Task Force of the PES, and an Editor of the IEEE TRANSACTIONS ON ENERGY CONVERSION. He holds two patents in power conversion for renewable energy.

Vahan Gevorgian (M'97) received Bachelor's and Ph.D. degrees in electrical engineering from Yerevan Polytechnic Institute, Yerevan, Armenia, in 1986 and 1993, respectively.

He is currently a Research Engineer with the National Renewable Energy Laboratory, Golden, CO, USA. His research interests include modeling various power systems with variable renewable generation and also testing and demonstrating grid integration aspects of various renewable energy technologies.

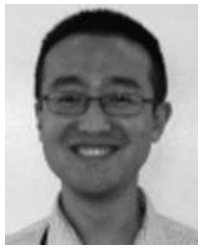

Yingchen Zhang (M'07) received the B.S.E.E. degree from Tianjin University, Tianjin, China, in 2003, and the Ph.D. degree in electrical engineering from Virginia Polytechnic Institute and State University, Blacksburg, VA, USA, in 2010.

He is currently with the National Renewable Energy Laboratory, Golden, CO, USA. His research interests include power system stability with large-scale integration of renewable energies, power system wide-area monitoring, and phasor measurement unit applications for renewable integrations.

Surya Santoso (M'96–SM'02) received the B.S. degree in electrical engineering from Satya Wacana Christian University, Salatiga, Indonesia, in 1992, and the M.S.E. and Ph.D. degrees in electrical engineering from the University of Texas at Austin, Austin, TX, USA, in 1994 and 1996, respectively, all in electrical engineering.

He was a Senior Power Systems and Consulting Engineer with Electrotek Concepts, Knoxville, TN, USA, from 1997 to 2003. He joined the faculty of the University of Texas at Austin as an Assistant Professor, in 2003, and since 2009, he has been an Associate Professor. His research interests include power quality, power systems modeling and simulation, and wind power integration.